JMEPEG (2012) 21:2572–2577
DOI: 10.1007/s11665-012-0366-1

1059-9495/$19.00

Characterization of Inclusions in VIM/VAR NiTi Alloys

A. Coda, S. Zilio, D. Norwich, and F. Sczerzenie

(Submitted March 16, 2012; in revised form August 1, 2012)

Inclusions content is important for the mechanical behavior and performances of NiTi-based products particularly in fatigue-rated devices. Higher inclusions content has been correlated to reductions in transformation temperatures and strain recovery under mechanical or thermo-mechanical cycling. Moreover, most fatigue fractures show inclusions at the initiation site. However, there is a general lack of information on the nature and characteristics of such inclusions, especially those typically recognized as intermetallics oxides. In this study, the common scanning electron microscopy technique has been used to investigate the chemistry and morphology of inclusions in commercial standard VIM/VAR binary NiTi alloys. The defined experimental procedure, results, and their significance will be presented and discussed.

Keywords biomaterials, electron microscopy, metallography

1. Introduction

It is well known in the metal industry that non-metallic inclusions are influenced primarily by the melting technique. At the present time, commercial NiTi alloys are produced by vacuum induction melting (VIM), vacuum arc melting (VAR), or a hybrid process where the primary VIM ingot is further refined using a VAR process (VIM/VAR) (Ref 1).

Inclusion content is a concern for nickel-titanium thermo-elastic alloys for fatigue-rated devices. Fatigue life is important for lower transformation temperature superelastic alloys for surgical implants in the human body (Ref 2). It is also important for higher transformation temperature thermally or electrically actuated devices for industrial applications (Ref 3). Most fatigue fractures show inclusions at the initiation site (Ref 4). Typically, in nickel-titanium alloys the inclusions are carbides, TiC, and intermetallic oxides, $Ti_4Ni_2O_x$.

Studying the inclusions in NiTi alloys prepared by a laboratory scale VIM furnace using a graphite crucible, Zhang et al. (Ref 5) detected eutectic TiC in an as-cast ingot with 200 ppm carbon. But for ingots with higher carbon content, both eutectic and primary TiC were present in the microstructure. Graham et al. (Ref 6). studied the inclusions in VAR NiTi alloys. The chemistry of inclusions was not analyzed but assumed to be $Ti_4Ni_2O_x$. Recent work by Toro et al. (Ref 7) characterized inclusions in NiTi tubing by both scanning electron microscopy (SEM) and optical metallography. They reported that both carbides and oxides are isolated particles in hot rolled vacuum induction melted and vacuum arc re-melted (VIM-VAR) bar. Nevertheless, there is a general lack of information on the nature and chemistry of such inclusions, especially those typically recognized as intermetallic oxides.

In Fig. 1, a secondary electron micrograph of a standard VIM-VAR NiTi alloy is reported. Three types of inclusions can be observed. In order to not anticipate any conclusion about the nature and the chemistry of such kind of particles, they were identified in the picture as black, gray (sometimes fractured), and black particles embedded in a gray particle.

The aim of this study is to provide further understanding on the inclusion identity of VIM/VAR NiTi alloys as well as a practical method to better analyze their chemistry by using SEM.

2. Experimental

Inclusion content was examined in two VIM-VAR alloys with different transformation temperatures (TTR) controlled by the Ni/Ti ratio. The alloys are designated by austenite start temperature, A_s, in the fully annealed condition (Ref 8). They varied from $A_s = -15$ °C (50.7 a/o Ni) to $A_s = +95$ °C (49.6 a/o Ni). This range of chemistry was chosen to assess the effect of Ni/Ti ratio on inclusion formation at 6.3 mm diameter hot rolled coil.

The samples were taken from head, center, and tail of full-size production coils. All the samples were prepared according to the standard metallographic specimen preparation procedure. Longitudinal centerline samples, as shown in Fig. 2, were ground in stages through 120 grit stone, 240 grit paper, and polished with 15 μm diamond, 9 μm diamond and finally 3 μm diamond.

The inclusion analysis was carried out by scanning the length of each sample in three regions of the cross section: the centerline, the mid-radius, and the near edge lines. Nine fields of view and over one hundred particles per sample were analyzed.

The NiTi samples were analyzed on a field emission (FE-SEM) microscope (Zeiss Supra 55 VP) equipped with

This article is an invited paper selected from presentations at the International Conference on Shape Memory and Superelastic Technologies 2011, held November 6-9, 2011, in Hong Kong, China, and has been expanded from the original presentation.

A. Coda, S. Zilio, SAES Getters S.p.A, Lainate, MI, Italy; **D. Norwich**, Memry Corporation, Bethel, CT; and **F. Sczerzenie**, SAES Smart Materials, New Hartford, NY. Contact e-mail: alberto_coda@saes-group.com.

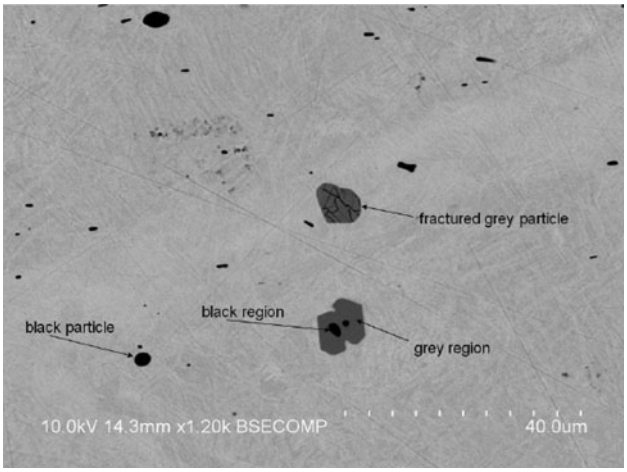

Fig. 1 Secondary electron micrograph of a standard VIM-VAR NiTi alloy

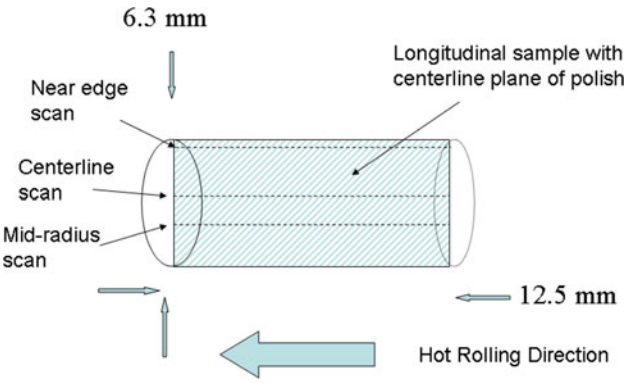

Fig. 2 Sketch of the metallographic longitudinal sample

Table 1 EDS optimized parameters used for the analyses

	Average analyses	Inclusion spot analyses (and maps)
Acceleration voltage, kV	20	5
Quantum optimization	Co standard	Si standard
Standardization	Standardless	Ni/Ti standardization at 5 kV using 20 kV results
Analysis area	1000× magnification	Spot (lines for maps)
Process time	4	6
Lifetime, s	40	80
Dead time, %	32	30
Working distance, mm	8	8

Inlens, secondary electron and backscatter electron detectors and with an energy dispersive x-ray (EDS) probe (Oxford INCA PentaFETx3) cooled with liquid nitrogen.

Preliminary average analyses were performed on a 1000× magnification area mainly to verify the Ni/Ti ratio in the sample (at least three analyses per sample were performed). The parameters are summarized in Table 1. The analyses were performed at 20 kV and 8 mm working distance (the ideal

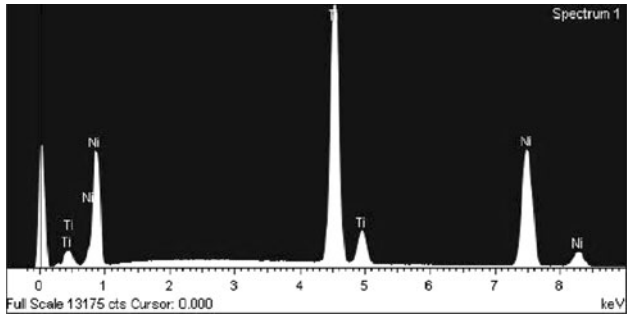

Fig. 3 Example of EDS spectrum of NiTi alloy matrix

conditions for the instrument), resulting in about 8-13 kcounts for the main peaks of Ni and Ti (see Fig. 3) for a lifetime (net analysis duration) of 40 s. Finally, a process time 4 (adimensional parameter proportional to the time to process a single photon on an instrument scale from 1 to 6) was used. Following the acceleration voltage, the Kα transitions (at 4.51 and 7.47 keV for Ti and Ni, respectively) were available for quantification. In this case, a Co standard was used for quantum optimization (energy and total current calibration). Every single element was quantified using the standardless method (factory calibration and software matrix correction, very suitable for EDS analyses).

Inclusion spot analyses and linescan maps were performed at higher magnifications. As the interaction volume related to the x-ray photon generation strongly depends on the acceleration voltage, lower voltage, i.e., 5 kV, was needed to minimize the influence of the matrix on the particle analyses.

The Monte Carlo simulation displayed in Fig. 4 gives an example of the interaction volume variation. Therefore, new parameters were used: to get at least 0.5-1 kcounts for Ni and Ti peaks a lifetime of 80 s was used. In addition, a process time of 6 was used to increase the resolution and to better separate the Ti and O peaks. As the generated photon amount was lower compared to the 20 kV analyses, the higher process time did not increase the pile-up phenomenon (counts having to be ignored because of being relative to two photons at the same time). It can be seen that the dead time is the same at about 30% for both 20 and 5 kV acceleration voltage which is ideal for the instrument.

In this case, a Si standard was used for quantum optimization because the Co Kα transitions were not measurable. At 5 kV, just the Lα transitions (at 0.45 and 0.85 keV for Ti and Ni, respectively) were available for quantification. So to improve the analysis for Ti and Ni, the Ni/Ti ratio was standardized during an average analysis at 5 kV using the more precise results obtained at 20 kV.

Finally, to take the pictures and to define the inclusion boundaries for the analyses, the secondary electron detector was used because of the better contrast compared to the backscatter detector at 5 kV. In Table 2, the interaction diameter for light and medium elements at 20 and 5 kV are summarized.

3. Results and Discussion

The procedure described in the previous section was used to quantify the compositions of the different inclusion species

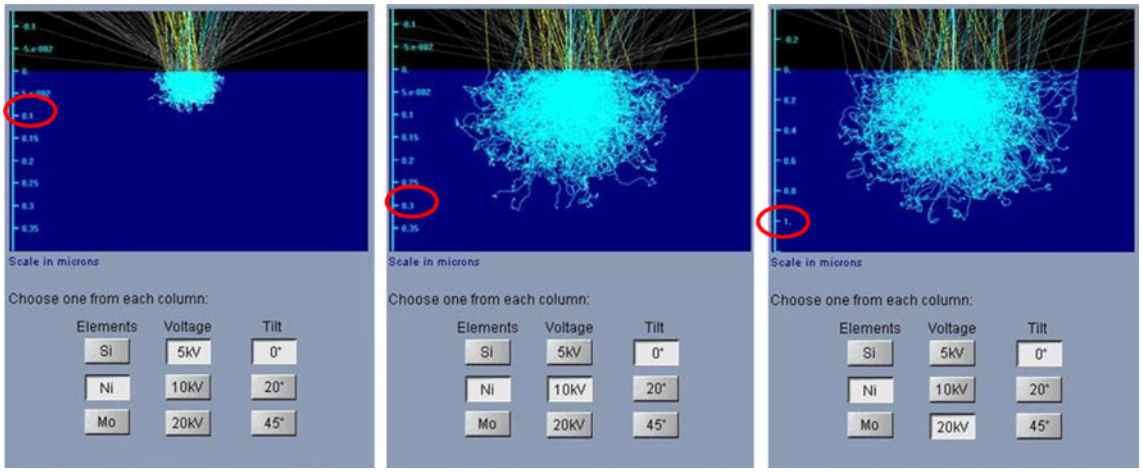

Fig. 4 Monte Carlo simulation of the interaction volume as function of the acceleration voltage. In red circles, the interaction depths 0.1, 0.3, and 1 μm at 5, 10, and 20 kV are highlighted, respectively (Color figure online)

Table 2 Interaction diameter at 20 and 5 kV for light and medium elements

	Acceleration voltage, kV	
	20	**5**
Interaction diameter for light elements (C, O), μm	10	0.8
Interaction diameter for medium elements (Ni, Ti), μm	3	0.3

detected in the two materials selected for this study. The results of EDS analyses are summarized in Table 3. For all the materials, both the compositions of the NiTi matrix and any inclusion species with the average concentration of each element detected by the microprobe are reported. The numbers in parentheses indicate the measured standard deviation and $<$LOD means that the concentration of such element is below the Limit of Detection (LOD).

As it can be seen, in standard superelastic Nitinol ($A_s = -15$ °C) three types of inclusions have been observed. The black particles are mainly based on titanium carbide (TiC) with a non-negligible amount of oxygen. The oxygen is usually present within the crystal lattice of TiC as a substitutional element (Ref 9). All the black particles analyzed showed nearly the same composition, but in particular, oxygen was consistently detected together with Ti and C. This kind of non-metallic inclusion will be indicated as TiC(O). As already pointed out by Toro et al., these particles are not complex oxide-carbide compounds, given that their structure is always cubic and compatible with that of TiC.

In Fig. 5(a), a secondary electron micrograph of a TiC(O) inclusion is reported. Both the EDS linescan map (see Fig. 5b) and spot analysis (see Fig. 5c) confirm the presence of mostly Ti, C, and O within the particle.

Ti, Ni, and O were detected as main elements of the gray particles. The average composition is Ti 58 at.%, Ni 27 at.%, and O 15 at.%. This stoichiometry would support the well-defined atomic ratio of mixed oxide Ti_4Ni_2O. In Fig. 6(a), a secondary electron micrograph of this kind of inclusion is shown. Also in this case the linescan across the particle (see Fig. 6b) and the spot analysis (in Fig. 6c) indicate the presence of such elements with a very good peak resolution. A very small carbon peak was also detected, but the linescan shows that the level is very close to the background and quantification is almost impossible. The presence of C within the inclusion can be reasonably excluded.

Gray particles with embedded black particles (named "core-shell" inclusion) represent the third family of inclusions detected in standard superelastic NiTi. As it is seen in Table 3, the core is made by titanium carbide, TiC(O), where the amount of substitutional oxygen is lower than in the isolated black particles. The shell composition can be associated to the intermetallic compound Ti_2Ni with both carbon and oxygen dissolved into the interstitial sites of its crystal lattice. We will indicate this part of the inclusion as Ti_2Ni(C, O). In Fig. 7(a), the secondary electron micrograph of one of such particles is displayed. From the picture, it is possible to easily recognize the black core and the gray shell. The EDS linescan, reported in Fig. 7(b), shows the evolution of the concentration across the particle for each element. It is evident the double drop of nickel concentration from the NiTi matrix to the core and the related increase of carbon and titanium. Oxygen appears to be stable and equally distributed within the particle. Also, the spot analyses carried out both in the gray (Fig. 7c) and black regions (Fig. 7d) of the inclusion confirm the compositions just described and discussed.

Even in the case of standard shape memory material ($A_s = +95$ °C), three types of inclusions have been detected. The EDS analyses showed that the nature and the composition of the dark and core-shell particles are TiC(O) and TiC(O)/Ti_2Ni(C, O), respectively, as already displayed for standard superelastic NiTi.

Again, it must be stressed that oxygen is concentrated within the carbides and core-shell inclusions. The unusual chemistry of such inclusions seems to suggest that titanium carbide in some way should be able to catalyze the oxides formation within the NiTi matrix. Still much work needs to be done to

Table 3 Summary of FESEM-EDS analyses results

Material	Condition	Zone	C, at.%	0, at.%	Ti, at.%	Ni, at.%
Standard VIM/VAR	$A_s = -15$ °C	Average (20 kV)	<LOD	<LOD	49.9 (0.05)	50.1 (0.05)
		Inclusion (dark)	32 (1)	15 (1)	53 (1)	<LOD
		Inclusion (gray)	<LOD	15 (1)	58 (1)	27 (1)
		Inclusion (dark core)	37 (1)	6 (1)	57 (1)	<LOD
		Inclusion (gray shell)	6 (1)	8 (1)	58 (1)	28 (1)
Standard VIM/VAR	$A_s = +95$ °C	Average (20 kV)	<LOD	<LOD	50.7 (0.05)	49.3 (0.05)
		Inclusion (dark)	37 (1)	6 (1)	57 (1)	<LOD
		Inclusion (gray)	<LOD	7 (2)	63 (1)	30 (1)
		Inclusion (gray)	<LOD	<LOD	65 (2)	35 (2)
		Inclusion (dark core)	38 (1)	4 (1)	58 (1)	<LOD
		Inclusion (gray shell)	5 (1)	7 (1)	60 (1)	28 (1)

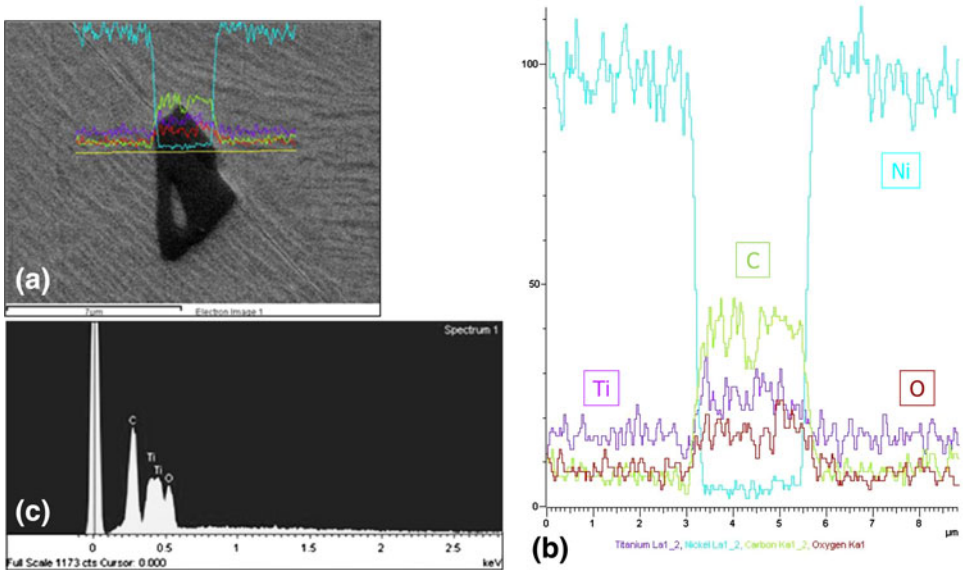

Fig. 5 (a) Secondary electron micrograph of a TiC(O) inclusion. (b) EDS linescan map across TiC(O) inclusion. (c) EDS spot spectrum of TiC(O) inclusion

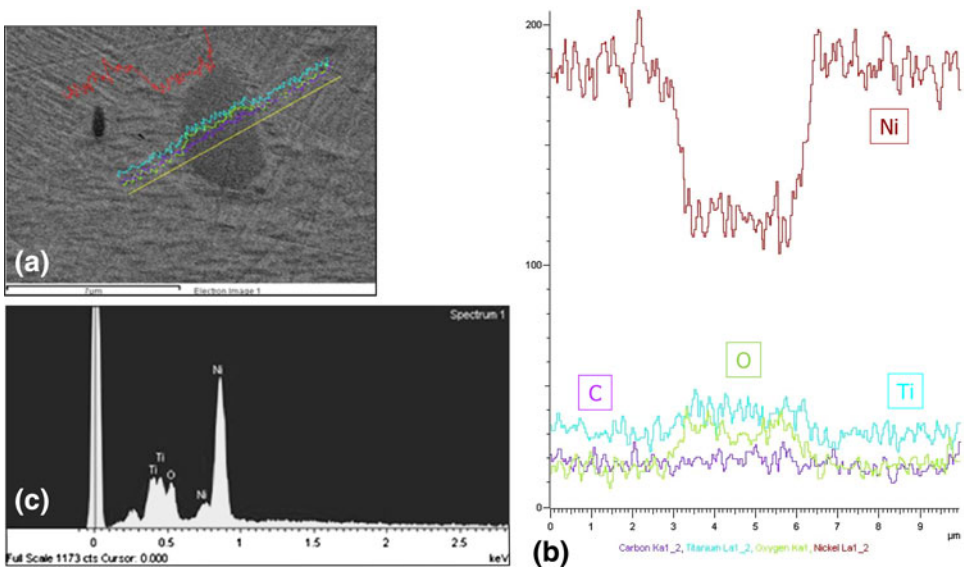

Fig. 6 (a) Secondary electron micrograph of a Ti_4Ni_2O inclusion. (b) EDS linescan map across Ti_4Ni_2O inclusion. (c) EDS spot spectrum of Ti_4Ni_2O inclusion

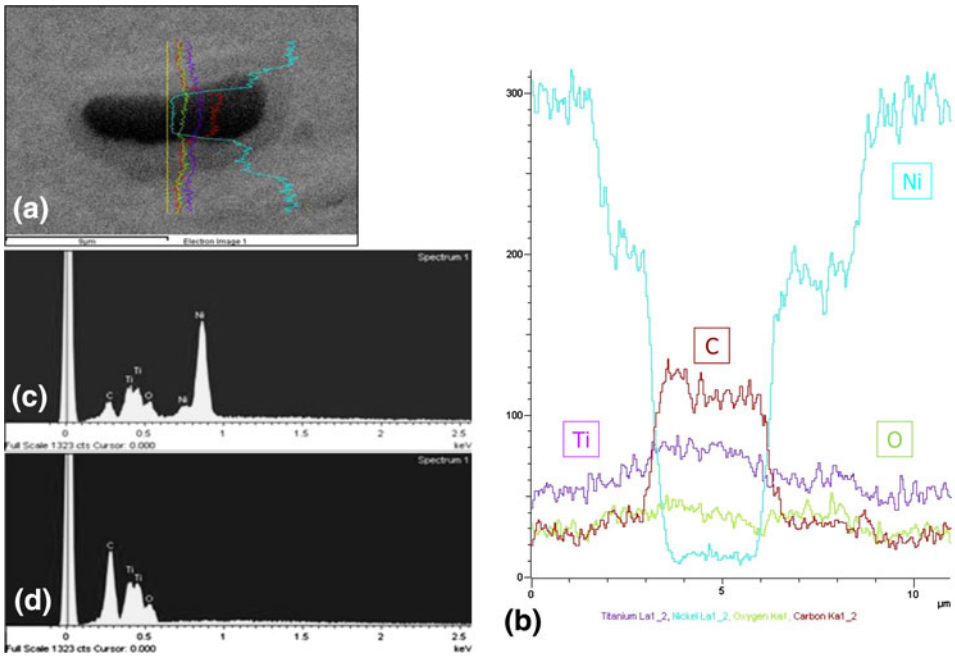

Fig. 7 (a) Secondary electron micrograph of a core-shell inclusion. (b) EDS linescan map across core-shell inclusion. (c) EDS spot spectrum of the gray (shell) region. (d) EDS spot spectrum of the black (core) region

better clarify the possible mechanism of this microstructural evolution.

A significant difference is given by the gray particles. In this case, looking at the average composition of such inclusions, it seems to be associated more to the intermetallic compound Ti_2Ni, with or without interstitial oxygen, indicated as $Ti_2Ni(O)$, rather than to the mixed oxide typically known as $Ti_4Ni_2O_x$. The presence of this intermetallic compound has been noticed not only in Ti-rich formulations but also in Ni-rich formulations. The reasons of such behavior were well explained by Frenzel et al. (Ref 10). They demonstrated that the volume fraction of Ti_2Ni precipitates is much larger in the Ti-rich alloys. Moreover, it is generally recognized that this intermetallic compound is easily stabilized by oxygen and can dissolve up to ~15 at.% (Ref 11, 12). When a small amount of oxygen is absorbed by many Ti_2Ni particles, as in Ti-rich material, the resulting oxygen concentration in each particle is low, and sometimes no oxygen peak is detected in the corresponding EDS spectra. When, in contrast, the same amount of oxygen is taken up by a much smaller number of particles, as in Ni-rich material, the oxygen concentration in each particle is high, a clear peak can be detected by the microprobe, and the formation of Ti_4Ni_2O compound can occur. It has to be underlined that Frenzel et al. are more inclined to consider these inclusions as Ti_2Ni precipitates with a high solubility for oxygen even at higher Ni concentrations. However, no crystallographic data of the lattice parameters supporting this hypothesis have been reported. In our opinion, even if the mechanism of Ti_2Ni stabilization by oxygen seems to be correct, the nature of such inclusions must be distinguished for Ti- and Ni-rich alloys. In shape memory NiTi alloys (Ti-rich), $Ti_2Ni(O)$ inclusions can be present often with a negligible amount of solubilized oxygen, whereas in superelastic NiTi alloys, the oxygen in Ti_2Ni is consistently recurring. In our experimental campaign, 100% of the analyzed particles showed a composition with Ni:Ti:O ratios of 4:2:1, which can be referred to as the well-characterized Ti_4Ni_2O oxide (Ref 13, 14).

4. Conclusions

1. A suitable FESEM-EDS procedure for inclusion analysis in NiTi alloys has been identified.
2. In VIM/VAR nitinol, four main types of inclusions can be distinguished:

   a. Titanium carbide TiC(O) with a significant amount of substitutional oxygen.
   b. Intermetallic oxide Ti_4Ni_2O with a well-defined stoichiometric ratio of the three elements.
   c. Ti_2Ni precipitates, with or without some interstitial oxygen. These particles were observed only in high temperature NiTi, due probably to their easier formation in Ti-rich formulation.
   d. Core-shell inclusions made by a core of TiC(O) and a shell of $Ti_2Ni(C,O)$. The unusual chemistry of these inclusions seems to suggest that titanium carbide should be able to catalyze the intermetallic oxide formation within the NiTi matrix in some way still unclear.

References

1. S.M. Russell, Nitinol Melting and Fabrication, *Proceedings of SMST 2000*, S.M. Russell and A.R. Pelton, Eds., 2000, p 1–9
2. N. Morgan et al., Carbon and Oxygen Levels in Nitinol Alloys and the Implications for Medical Device Manufacture and Durability, *Proceedings of SMST 2006*, B. Berg, M.R. Mitchell, and J. Proft, Eds., 2006, p 821–828

3. M. Mertmann, Fatigue in Nitinol Actuators, *Proceedings of ACTUATOR 2006*, 2006, p 461–466
4. M. Reinoehl et al., The Influence of Melt Practice on Final Fatigue Properties of Superelastic NiTi Wires, *Proceedings of SMST 2000*, S.M. Russell and A.R. Pelton, Eds., 2000, p 397–403
5. Z. Zhang et al., Orientation Relationship Between TiC Carbides and B2 Phase in As-Cast and Heat Treated NiTi Shape Memory Alloys, *Mater. Sci. Eng., A*, 2006, **438–440**, p 879–882
6. R. Graham et al., Characteristics of High Purity Nitinol, *Proceedings of SMST 2003*, A.R. Pelton and T. Duerig Eds., 2003, p 7–14
7. A. Toro et al., Characterization of Non-Metallic Inclusions in Superelastic NiTi Tubes, *J. Mater. Eng. Perform.*, 2009, **18**(5–6), p 448–458
8. ASTM International, F2004-05, Annual Book of ASTM Standards, vol. 13.01
9. International Centre for Diffraction Data (www.icdd.com), Newton Square, Pennsylvania, Release 2005
10. J. Frenzel et al., Influence of Ni on Martensitic Transformations in NiTi Shape Memory Alloys, *Acta Mater.*, 2010, **58**, p 3444–3458
11. M.V. Nevitt, Stabilization of Certain Ti_2Ni-Type Phases by Oxygen, *Trans. Met. Soc. AIME*, 1960, **218**(2), p 327–331
12. V.G. Chuprina and I.M. Shalya, Reactions of TiNi with Oxygen, *Powder Metall. Met. Ceram.*, 2002, **41**, p 85–89
13. M.H. Muller and H.W. Knoff, The Crystal Structures of Ti_2Cu, Ti_2Ni, Ti_4Ni_2O, and Ti_4Cu_2O, *Trans. Met. Soc. AIME*, 1963, **227**, p 674–678
14. R. Mackay et al., New Oxides of the Filled-Ti_2Ni-Type Structure, *J. Alloys Compd.*, 1994, **204**, p 109–118